Microscopy and Microanalysis (2021), **27**, 250–256
doi:10.1017/S1431927621000052

Microscopy AND Microanalysis

Original Article

In situ TEM Characterization of Microstructure Evolution and Mechanical Behavior of the 3D-Printed Inconel 718 Exposed to High Temperature

Supriya Koul[1], Le Zhou[1,2,3], Omar Ahmed[1], Yongho Sohn[1,2], Tengfei Jiang[1] and Akihiro Kushima[1,2,4]*

[1]Department of Materials Science and Engineering, University of Central Florida, Orlando, FL, USA; [2]Advanced Materials Processing and Analysis Center, University of Central Florida, Orlando, FL, USA; [3]Department of Mechanical Engineering, Marquette University, Milwaukee, WI 53233, USA and [4]NanoScience Technology Center, University of Central Florida, Orlando, FL, USA

Abstract

This *in situ* transmission electron microscopy work presents a nanoscale characterization of the microstructural evolution in 3D-printed Inconel 718 (IN718) while exposed to elevated temperature and an associated change in the mechanical property under tensile loading. Here, we utilized a specially designed specimen shape that enables tensile testing of nano-sized thin films without off-plane deformations. Additionally, it allows a seamless transition from the *in situ* heating to tensile experiment using the same specimen, which enables a direct correlation of the microstructure and the mechanical property of the sample. The method was successfully used to observe the residual stress relaxation and the formation of incoherent γ′ precipitates when temperature was increased to 700°C. The subsequent *in situ* tensile test revealed that the exposure of the as-printed IN718 to a high temperature without full heat treatment (solutionizing and double aging) leads to loss of ductility.

Key words: additive manufacturing, heat treatment, *in situ* transmission electron microscopy, IN718, nanoscale mechanics

(Received 27 August 2020; revised 14 January 2021; accepted 22 January 2021)

Introduction

Additive manufacturing (AM), commonly referred to as 3D printing, is expected to be a game-changer for the manufacturing industry (Aydinöz et al., 2016). The advancement of AM processes such as laser powder-bed fusion (LPBF) enables direct 3D printing of metal alloys. The LPBF method uses a scanning laser to melt or sinter (cohesive bonding) a powder-bed layer-by-layer to create complex and intricate three-dimensional geometries (Zhang et al., 2015). This technology, compared to conventional manufacturing methods, has advantages such as design flexibility, thus evading the limiting factors such as production quantity, lead-time, and dimensions (Wang et al., 2012; Aydinöz et al., 2016; Trosch et al., 2016; Kuo et al., 2017*b*).

Several studies have been conducted to compare the mechanical properties of materials produced by LPBF and the traditional production methods involving casting and thermo-mechanical working (Wang et al., 2012; Zhang et al., 2015; Trosch et al., 2016; Kuo et al., 2017*a*). The distinct melting/solidification dynamics of LPBF is one of the biggest challenges in successfully implementing the AM technology. LPBF involves rapid heating and cooling, and together with the small laser spot size, it leads to the formation of nonequilibrium phases with characteristic microstructures (Kelly & Kampe, 2004; Mumtaz et al., 2008; Thijs et al., 2010; Song et al., 2015; Li et al., 2016). Additionally, the microstructure of the LPBF-produced alloys can vary within the built sample (Baufeld et al., 2010; Thijs et al., 2015) because of the variation in the cooling rate from the rapid cooling of the melt pool at the top part to the slow-cooled region at the lower part (or the region processed at the earlier stage). It is also highly dependent on the build direction. Columnar grains are commonly observed along the build direction in the LPBF alloys (Amato et al., 2012; Vilaro et al., 2012; Mostafa et al., 2017) causing anisotropy in the mechanical properties (Zhao et al., 2008; Frazier, 2014; Song et al., 2015; Strößner et al., 2015; Deev et al., 2016). To achieve the desirable mechanical properties and thus meet the design specifications, the control of the microstructure by adequate solution heat treatment and aging is crucial (Zhou et al., 2019). There are many parameters that affect the microstructure and, consequently, the mechanical properties of the LPBF-produced alloys. This includes, but is not limited to, laser power and spot sizes, scan speed and direction, hatch spacing, and slice thickness, to name a few. By changing these parameters, the microstructure and the mechanical properties can be altered even for the same alloy composition. And the post-production heat treatment gives additional parameters leading to the fabrication of materials with a wide range of ductility and mechanical strengths (Ding et al., 2016). It is extremely challenging to optimize the entire processing route in order to achieve the

*Author for correspondence: Akihiro Kushima, E-mail: kushima@ucf.edu

Cite this article: Koul S, Zhou L, Ahmed O, Sohn Y, Jiang T, Kushima A (2021) *In situ* TEM Characterization of Microstructure Evolution and Mechanical Behavior of the 3D-Printed Inconel 718 Exposed to High Temperature. *Microsc Microanal* **27**, 250–256. doi:10.1017/S1431927621000052

target properties. Understanding the fundamental mechanism of the microstructure development and accompanying mechanical properties are essential for the efficient development of the LPBF processes. However, the knowledge and experience from conventionally manufactured alloys may not be directly applicable to LPBF alloys due to the difference in the microstructure.

There have been numerous studies comparing LPBF and the traditional production methods, such as casting and thermo-mechanical working (Wang et al., 2012; Zhang et al., 2015; Trosch et al., 2016; Kuo et al., 2017*a*), and investigating the effect of the heat treatment on the microstructures and the mechanical properties of the LPBF alloys (Song et al., 2012, 2014; Vrancken et al., 2012; Chlebus et al., 2015; Li et al., 2015, 2016; Zhang et al., 2015; Ter Haar et al., 2016; Tucho et al., 2017; Zhou et al., 2019). Components manufactured using LPBF can achieve mechanical properties close to those of the conventional techniques or even better. However, mechanical properties of the as-printed alloys may not satisfy the requirement of the highly demanding applications because of their characteristic microstructures. For example, due to the rapid heating and cooling cycles of the LPBF process, solute partitioning is prevalent, leading to micro-segregation and subsequent formation of brittle intermetallics such as Laves phase (Tucho et al., 2017). Here, post-production heat treatment is the key to enhancing the uniform elemental distribution and improving mechanical properties by promoting the precipitation of strengthening phases while eliminating the segregation of undesired phases (Zhang et al., 2015; Tucho et al., 2017).

Such postproduction heat-treatment studies have been well established for the bulk samples produced by conventional techniques, but limited information is available for powder-bed AM-processed samples (Zhang et al., 2018; Sing et al., 2020; Tsai et al., 2020). The LPBF-produced alloy may undergo a different structural evolution because its initial characteristic microstructure is different from those produced by the conventional routes. It is reported that during laser manufacturing of the IN718, the alloying elements, especially niobium (Nb) and molybdenum (Mo), tend to segregate in the inter-dendritic/cellular region compared to the conventionally produced alloys (Tucho et al., 2017). An enormous number of research works have been documented in the study of heat treatment and its relation to the deformation behavior in metallic structures. In the literature, several experimental and theoretical investigations account for analyzing the mechanical behavior of the bulk sample (de Formanoir et al., 2019; Hilaire et al., 2019; Sing et al., 2020). Meanwhile, there are only a handful of studies on the LPBF-printed alloys at the submicron scale (Liu et al., 2018; Shen et al., 2018; Bär et al., 2019).

Since the LPBF alloy has unique microstructures that vary within the material, fine-scale analysis is necessary to fully understand their mechanical properties. Here, *in situ* transmission electron microscopy (TEM) and scanning electron microscopy (SEM) experiments have been widely used to capture the deformation and the fracture mechanics in the materials at nano- and atomic scales (Rao et al., 2003; Haque & Saif, 2004; Zhu & Espinosa, 2005; Greer & Nix, 2006; Kiener & Minor, 2011; Kushima et al., 2012; Imrich et al., 2015; Wang et al., 2015). For example, compressive tests of additively-manufactured micro-pillars with several microns of diameter can be performed inside an SEM to analyze the force–deformation responses (Daryadel et al., 2019). Additionally, nanoindentation combined with SEM has been employed to study the mechanical properties of the LPBF-produced alloys and their spatial variations associated with the difference in the microstructures (Legros et al., 2011). The technique allows the quantitative evaluation of the mechanical properties of the very fine micro-phases found in the LPBF.

On the other hand, *in situ* TEM provides direct observations of the intrinsic deformation mechanisms and their relationships with the microstructures at higher spatial resolutions. It allows the characterization of the nanostructures within the micro-phases and analysis of their effects on the mechanical properties through real-time observation of the dynamic processes during mechanical deformations. The *in situ* TEM techniques have been used to investigate structural changes in materials during heating (Liu et al., 2015; Wang & Haque, 2015; Rao et al., 2017; Callisti et al., 2018; Topping et al., 2018; Albu et al., 2020) as well as deformation mechanisms at nano- and atomic scales (Haque & Saif, 2004; Zhu et al., 2005; Kiener & Minor, 2011; Wang et al., 2015). Various *in situ* TEM mechanical testing methods were developed in the past decade, including nanocompression on focused ion beam (FIB) microfabricated pillars (Shan et al., 2008), bending tests using electric field-induced resonance (Wang et al., 2008), and microelectromechanical systems (MEMS) based on lithography for performing *in situ* TEM straining experiments (Wang & Haque, 2015). MEMS fabrication technology of a freestanding tensile specimen with the force sensor and actuation mechanism for the force/displacement measurement shows distinct capabilities (Haque & Saif, 2004). The applications of these techniques have been explored with tremendous interest. For example, Minor et al. investigated the onset of plasticity using a miniature capacitive load–displacement transducer equipped on the TEM holder (Minor et al., 2006), and Liu et al. in their work revealed the effect of the dislocation network formed during selective laser melting on the dislocation motion by *in situ* TEM analysis using a straining holder (Liu et al. 2018).

These capabilities of the *in situ* TEM/SEM are important for establishing a fundamental understanding of the LPBF-produced alloys. In fact, several recent studies employed these techniques to study the AM process and the materials. The rapid solidification process of polycrystalline aluminum was observed by TEM using an ultrahigh frame-rate CCD camera with single-electron detection sensitivity (McKeown et al., 2016; Zweiacker et al., 2016). Microstructure evolutions during the postprocess heating of the AM materials were investigated by *in situ* TEM for Ni-based superalloy (Deshpande et al., 2020), Ti-alloy (Li et al., 2021), and Al-alloy (Albu et al., 2020). For the mechanical properties of AM-produced materials, the effect of the microstructure on the strength (Wu et al., 2016; Liu et al., 2018; Lin et al., 2019) and fatigue behavior (Wang et al., 2019) was studied by *in situ* TEM/SEM. However, performing *in situ* heating and mechanical tests on the exact same specimen to directly link the structural evolution and the mechanical property is still a challenging task.

Experimental Methodology

In this work, a unique *in situ* TEM procedure was developed to evaluate the microstructure evolution of LPBF-produced metal alloys when exposed to a high temperature and its effect on the mechanical property. This real-time experiment provides important insights regarding the evolution of the microstructure at different heating conditions and how the associated changes in the microstructures affect the mechanical properties. One of the

https://doi.org/10.1017/S1431927621000052 Published online by Cambridge University Press

biggest challenges during the *in situ* testing is maintaining the mechanical integrity because nanoscale samples are so thin. A significant amount of stress accumulates while thinning down using a FIB, which makes the sample intrinsically more fragile. This challenge is further complicated by leveling the thin testing sample onto the tensioning mechanism to ensure that the pure tension is applied to the sample. Otherwise, other forces such as torsion or bending may occur in addition to the tension. The fundamental principle is to measure the displacement of the tensile sample accurately (Zhu & Espinosa, 2005). Additionally, even a slight misalignment in the specimen orientation and loading direction can result in unaccounted flexural stresses on the specimen (Haque & Saif, 2002). Therefore, in order to seamlessly observe the change in the microstructure during heating and to conduct the mechanical test on the exact same sample inside the TEM, we designed a push-to-pull TEM sample configuration as shown in Figure 1. With the two ribs at the ends of the thin center part, off-plane motions such as bending and twisting of the film are restricted. When a pushing force is applied on the protruding part on one of the ribs with the thinned root, the rib bends away from the support on the other side of the center lamella, and the pushing force is converted into the tensile load on the center of the specimen. Because the off-plane motions are constrained by the ribs, a tensile deformation of the observation area can be achieved without undesired bending and twisting. Here, a notch was introduced as a stress concentration site to nucleate a crack and initiate the fracture, since it is very difficult to observe a specific feature at high magnification (Wang & Haque, 2015). A finite element analysis was conducted to confirm that the offset of the force does not affect the stress distribution at the crack tip (see Supplementary Material for details).

A specimen block with dimensions of 5 μm × 2 μm × 2 μm was cut from a LPBF-produced alloy and shaped by FIB using a FEI 200 TEM FIB to the push-to-pull geometry as shown in Figure 1. The detailed procedure is explained in Supplementary Figure S4. FIB current was carefully controlled to minimize the beam damage that may affect the mechanical property of the specimen (Kiener et al., 2007). The sample was heated inside the TEM using a heating holder (Gatan Model 652) for residual stress relaxation; the heated sample was then transferred to a 3D-nanomanipulation holder (Hummingbird Scientific) for tensile testing. A tungsten probe was used to apply the quasi-static displacement on the freestanding end of the FIB-prepared end of the specimen.

IN718 fabricated by LPBF was used as the subject of the study. The pre-alloyed IN718 gas-atomized powder with a diameter ranging from 10 to 45 μm was built into cubic samples by scanning laser manufacturing (SLM) 125HL LPBF unit. A laser beam of 200 W at a scanning speed of 900 mm/s in an argon atmosphere was used to fuse the powder particles. The details are recorded elsewhere (Zhou et al., 2019). First, an *in situ* heating experiment was conducted to confirm that the microstructure evolution can be captured with our setup. A thin TEM specimen was prepared using FIB. The specimen was mounted on the *in situ* heating holder, and the temperature was raised inside the TEM to analyze the nucleation and the growth of precipitates (γ', γ''). First, the temperature was increased from room temperature (~20°C) to 600°C at a heating rate of 50°C/min. The increase in temperature caused a sudden drift due to thermal expansion. After the drift was stabilized for 20 min, the temperature was raised to 700°C at a slower rate of 10°C/min.

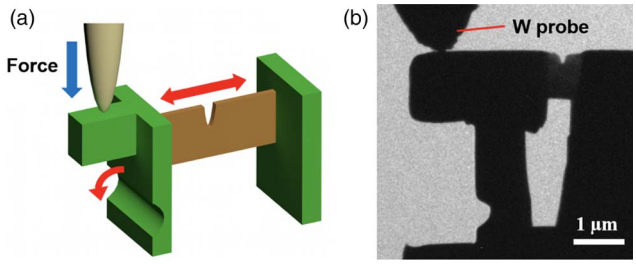

Fig. 1. (**a**) Schematic illustration of the push-to-pull sample configuration proposed in this work and (**b**) a TEM micrograph of the specimen prepared from scanning laser manufacturing-produced IN718.

Results and Discussion

Microstructural Evolution under Heating

Figure 2 shows the structural evolution of precipitates while heating (see also Supplementary Movie 1). The as-printed IN718 sample had a significant amount of residual stress due to fast heating/cooling processes in SLM. As the sample was heated, the stress was relieved (ii–iv) and the strain contrast was no longer visible at 640°C (iv). At 680°C, small precipitates began to nucleate in the matrix as indicated by the arrowheads (v). As the temperature increased, the precipitates continued to nucleate and grow introducing local strains in the material as shown in (vi). Electron diffraction patterns before and after the heating experiment were analyzed to confirm that the precipitates were γ' and γ'' phases (see Supplementary Figs. 6 and 7). Furthermore, increasing the temperature to 800°C (at a rate of 10°C/min) resulted in the formation of a needle-like δ-phase (see Supplementary Fig. 5(d)). However, no Laves phases were found in our study, which agrees with Amato et al. (2012). γ'' phase is metastable which transforms into δ-phase with similar composition and acicular structure at high temperature. This acicular δ-phase conversion reaction is accelerated around 800°C and would be highly undesirable because of the δ-phase embrittlement. The amount of δ-phase that formed in the sample was comparatively low because the IN718 alloy studied in this work has Nb in the range of 4.75–5.50 wt%, while it should be more than 7% for significant distributions of δ-phase (Zhang et al., 2010; Kuo et al., 2017*a*, 2017*b*). The above observations indicate that the microstructure evolution of the IN718 at high temperature can be captured within a thin TEM specimen used in this work.

Deformation and Fracture Behavior

To analyze the effect of the microstructure evolution on the mechanical properties, two specimens were cut from a single grain in as-printed IN718 within a few micrometers of each other and shaped into the push-to-pull samples as shown in Figure 1. Here, the tungsten probe was pushed against the sample at a displacement rate of 1.0 nm/s to apply tension to the thin observation area. Figure 3 shows the fracture process observed for the IN718 sample before heating (see also Supplementary Movies 3 and 4). Tensile deformation was successfully applied to the observation area, and the fracture process was captured. As the tension was applied to the specimen, the notch started to open wider (Figs. 3a and 3b). When further strain was imposed, a crack slowly nucleated from the surface as indicated by the arrowhead (Fig. 3c). Then, the crack started to open and propagated through the specimen (Figs. 3d–3f). At the latter

https://doi.org/10.1017/S1431927621000052 Published online by Cambridge University Press

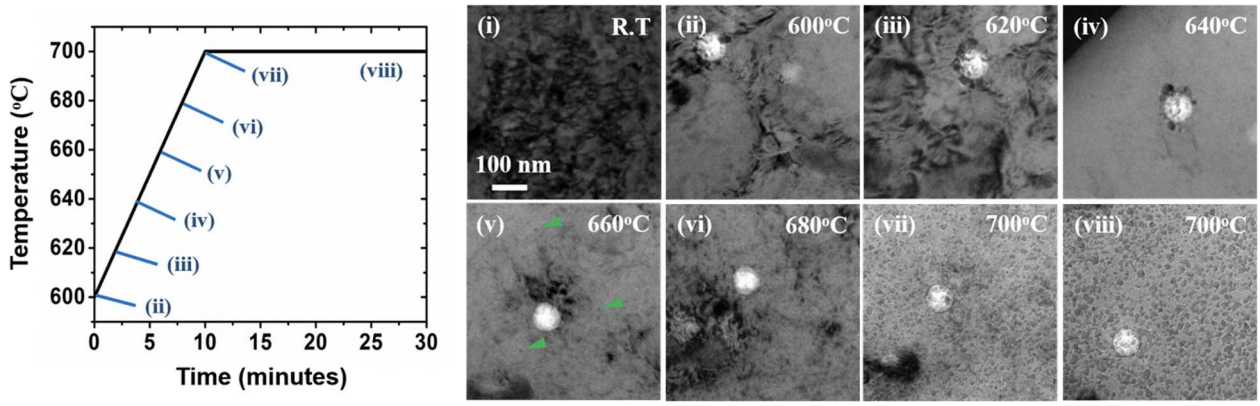

Fig. 2. Temperature change and the corresponding microstructure evolution of SLM-produced IN718 during *in situ* heating experiment. The sample morphology at room temperature before heating is shown in (i) as a reference. The residual stress in the as-produced sample was relaxed (ii, iii) and completely removed at 640°C (iv). At 660°C, precipitates started to nucleate as indicated by the arrowheads (v) accompanying local stresses as can be seen from the strain contrast. More precipitates nucleated and grew as the temperature was increased (vi, vii). When the sample was held at 700°C, the precipitates were uniformly distributed in the sample and the stress had been relaxed (viii).

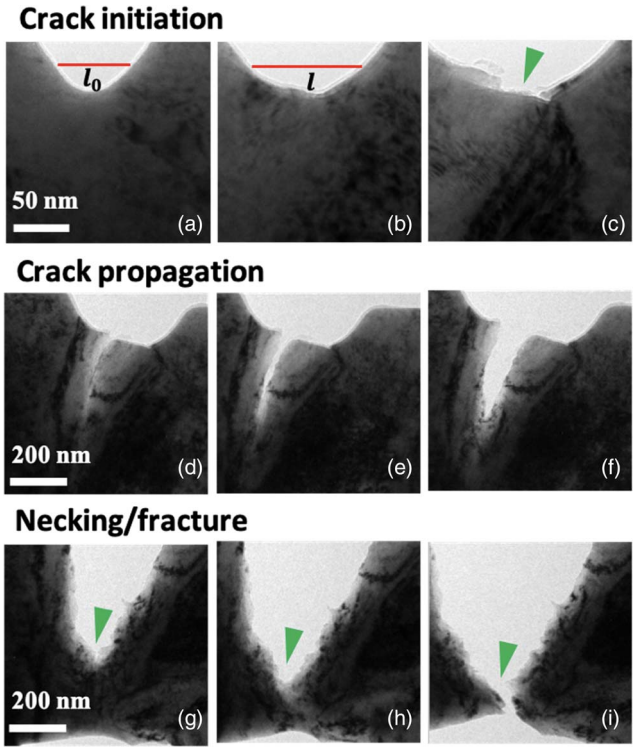

Fig. 3. Sequential TEM images of the fracture process of as-printed IN718: (**a–c**) crack initiation, (**d–f**) propagation, and (**g–i**) necking to ductile fracture.

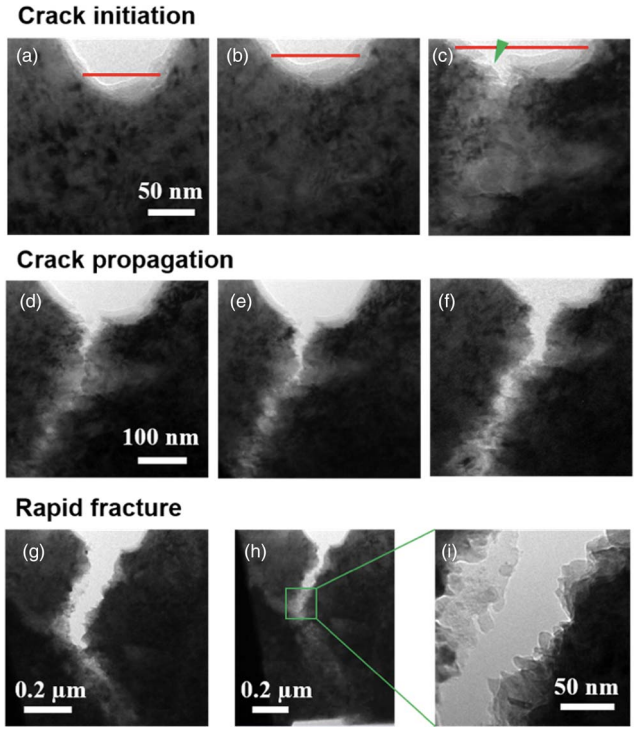

Fig. 4. Sequential TEM images of the fracture process of SLM-produced IN718 after exposure to elevated temperature inside TEM: (**a–c**) crack initiation, (**d–f**) propagation, and (**g–i**) rapid cleavage fracture.

stage of the deformation just before the fracture (Figs. 3g–3i), necking was observed, indicating a ductile fracture. After heating to 800°C in a same manner as described above (direct heating in TEM), the fracture process of the specimen showed completely different behavior as shown in Figure 4 (see also Supplementary Movies 5 and 6). A crack initiated from the notch at much smaller strain compared to the as-printed sample (Figs. 4a–4c). Once the crack was nucleated, it propagated rapidly across the specimen (Figs. 4d–4f) and led to the final fracture (Fig. 4g). The specimen showed no necking after the fracture (Fig. 4h), and the higher magnification images of the rough fracture surface indicated that the process was brittle.

As a comparison, a push-to-pull tensile specimen was cut from the "fully heat-treated" IN718 (Zhou et al., 2019). It was solution heat-treated at 1,065°C for 1 h followed by the two-step aging at 720°C for 8 h and 650°C for 7 h, with γ'/γ'' precipitates coherent with the γ matrix. This sample, hereafter, is referred to as fully heat treated (FHT). As shown in Figure 5, the deformation behavior was different from the as-printed and directly heated specimen as discussed above. At the initiation stage, a network of nano-sized cracks was formed near the notch, forming 5–10 nm grains in the region marked by the dashed square (Fig. 5b). The detailed view of the crack nucleation site is shown in Supplementary Figure 8. The size of the grains matches well with the coherent

https://doi.org/10.1017/S1431927621000052 Published online by Cambridge University Press

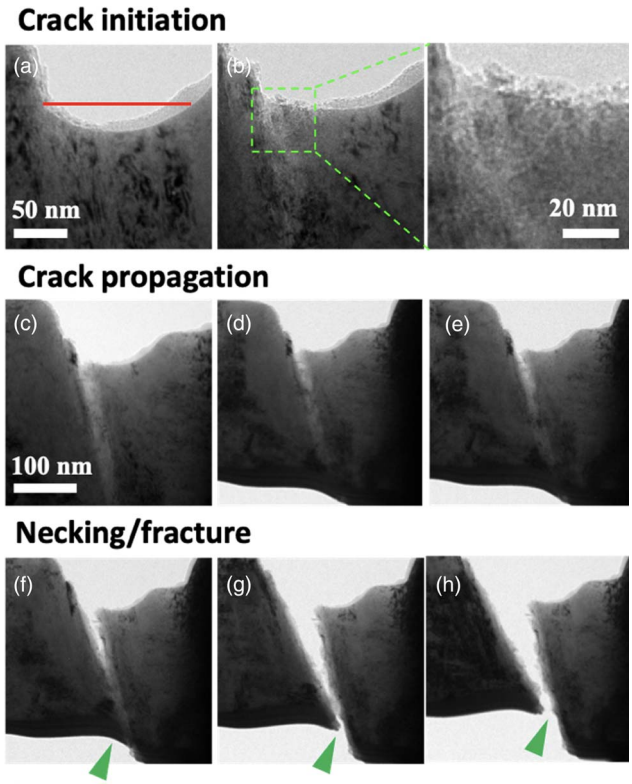

Fig. 5. Sequential TEM images of the fracture process of SLM-produced IN718 after solutionizing and aging: (**a,b**) crack initiation, (**c–e**) propagation, and (**f–h**) ductile fracture.

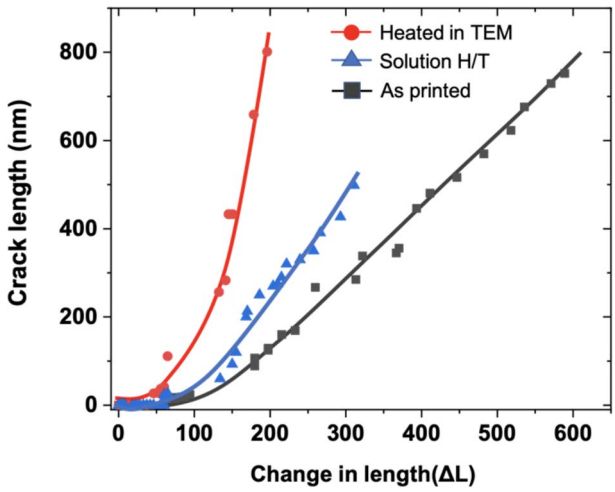

Fig. 6. Relationships between crack length and the notch opening of the IN718 specimen produced by SLM: as-printed (square), heated in TEM holder (circle), and solution heat treated (triangle).

γ′ and γ″ precipitates. As the tension continued, the crack propagated rapidly (Figs. 5c–5e). However, it did not lead to a complete fracture as in the directly heated specimen. Instead, it showed necking before the fracture as indicated by the arrowheads (Figs. 5f–5h). These results demonstrate the important correlation between heat treatment, microstructural constituents (i.e., γ′/ γ″ precipitates and δ-phase), and mechanical properties (i.e., strength, ductility, and fracture toughness). To quantify the ductility of the LPBF-produced IN718 before heating (i.e., as-built), after direct heating, and the proper two-stage heat treatment, the relationship between the crack length and the notch opening was analyzed. The initial notch size l_0 is indicated by the solid lines as shown in Figures 3a, 4a, and 5a. The features in the samples were tracked to determine the evolution of the notch size and the crack length. Figure 6 shows the relationship between the crack length and the notch opening, $\Delta l = l - l_0$. (Relationships between crack length, notch opening, and the displacement of the indentor are shown in Supplementary Fig. S9.) The crack developed slowly for the as-printed sample, and the length increased linearly as the notch opened. The directly heated sample showed a rapid increase in the crack length at a much smaller notch opening that corresponded to the brittle fracture. On the other hand, the crack length increased slowly for the FHT sample during its propagation, showing a ductile behavior. While both directly heated and FHT samples improved their strength due to the precipitation hardening, only the latter specimen with coherent precipitates maintained its toughness. Since the specimen was prepared from a single grain, the samples tested were single crystal. Therefore, the effect of needle-like δ-phase segregation at the grain boundary that restricts the dislocation motion (Trosch et al., 2016; Kuo et al., 2017*a*) was not present in the as-printed IN718 specimen. This enables dislocations to propagate freely and allows easy gliding of the crystallographic planes leading to the ductile deformation (see Supplementary Fig. S10). On the other hand, the abrupt fracture at the lower strain in the sample after direct heating to 800°C is attributed to the improper heat treatment, which caused a segregated formation of precipitates leading to several nucleation sites for catastrophic failure (Zhou et al., 2019). Here, the embrittling precipitates formed in the specimen after heating causes dislocation pinning, which restricts the sliding of the crystallographic planes and causes brittle fracture. A similar ductile-to-brittle transition from the as-printed IN718 alloy after heating was reported for the bulk specimen (Popovich et al., 2017). The reason attributed to this behavior was the large amount of needle-like δ precipitates and undissolved Laves phases. Our observation demonstrated that the matrix grain itself also loses ductility as incoherent γ′/ γ″ phases precipitate.

Conclusion

Great attention has been paid to LPBF production and postproduction heat treatment parameters to produce desired microstructure and eliminate pores. Our observation confirms that as-printed IN718 is less suited for high-temperature applications, and that a simple postprint heating (e.g., direct heating) cannot ensure its mechanical properties. However, further improvements may be possible by tailoring the nanostructures within the grains. For example, the hardness of the LPBF-produced IN718 was improved by the precipitation of coherent γ′ and γ″ precipitates following the full heat treatment (Zhang et al., 2010; Kuo et al., 2017*b*; Zhou et al., 2019). An effectively homogenizing solution treatment is necessary for subsequent precipitation hardening to properly take place while preventing the microsegregation of incoherent precipitates within the grains that lead to the embrittlement of LPBF-produced IN718. Although this work focused on LPBF-produced IN718 alloy and evaluated the relationships between microstructural evolution and the mechanical properties, the unique technique developed in this work is not restricted to the field of LPBF, but can be widely used to study the mechanical

https://doi.org/10.1017/S1431927621000052 Published online by Cambridge University Press

behavior of materials, including ceramics, biomaterials, and semiconductors, where the relationship among processing, nano/micro-structure, and mechanical properties elucidates the performance of engineered components and systems.

Supplementary material. To view supplementary material for this article, please visit https://doi.org/10.1017/S1431927621000052.

Acknowledgments. L.Z. and Y.S. acknowledge the financial support, in part by the Office of Naval Research (No. N00014-17-1-2559), and in part by the U.S. Army Research Laboratory (No. W911NF1720172). The views, opinions, and conclusions made in this document are those of the authors and should not be interpreted as representing the official policies, either expressed or implied, of the Office of Naval Research or the U.S. Army Research Laboratory or the U.S. Government.

References

Albu M, Krisper R, Lammer J, Kothleitner G, Fiocchi J & Bassani P (2020). Microstructure evolution during in-situ heating of AlSi10Mg alloy powders and additive manufactured parts. *Addit Manuf* **36**, 101605.

Amato KN, Gaytan SM, Murr LE, Martinez E, Shindo PW, Hernandez J, Collins S & Medina F (2012). Microstructures and mechanical behavior of Inconel 718 fabricated by selective laser melting. *Acta Mater* **60**(5), 2229–2239.

Aydinöz ME, Brenne F, Schaper M, Schaak C, Tillmann W, Nellesen J & Niendorf T (2016). On the microstructural and mechanical properties of post-treated additively manufactured Inconel 718 superalloy under quasi-static and cyclic loading. *Mater Sci Eng A* **669**, 246–258.

Bär F, Berger L, Jauer L, Kurtuldu G, Schäublin R, Schleifenbaum JH & Löffler JF (2019). Laser additive manufacturing of biodegradable magnesium alloy WE43: A detailed microstructure analysis. *Acta Biomater* **98**, 36–49.

Baufeld B, Biest OVd & Gault R (2010). Additive manufacturing of Ti–6Al–4 V components by shaped metal deposition: Microstructure and mechanical properties. *Mater Des* **31**, S106–S111.

Callisti M, Tichelaar FD & Polcar T (2018). In situ TEM observations on the structural evolution of a nanocrystalline W-Ti alloy at elevated temperatures. *J Alloys Compd* **749**, 1000–1008.

Chlebus E, Gruber K, Kuźnicka B, Kurzac J & Kurzynowski T (2015). Effect of heat treatment on the microstructure and mechanical properties of Inconel 718 processed by selective laser melting. *Mater Sci Eng A* **639**, 647–655.

Daryadel S, Behroozfar A & Minary-Jolandan M (2019). A microscale additive manufacturing approach for in situ nanomechanics. *Mater Sci Eng A* **767**, 138441.

Deev AA, Kuznetcov PA & Petrov SN (2016). Anisotropy of mechanical properties and its correlation with the structure of the stainless steel 316L produced by the SLM method. *Phys Procedia* **83**, 789–796.

de Formanoir C, Martin G, Prima F, Allain SYP, Dessolier T, Sun F, Vivès S, Hary B, Bréchet Y & Godet S (2019). Micromechanical behavior and thermal stability of a dual-phase α+α' titanium alloy produced by additive manufacturing. *Acta Mater* **162**, 149–162.

Deshpande A, Deb Nath S, Atre S & Hsu K (2020). Effect of post processing heat treatment routes on microstructure and mechanical property evolution of Haynes 282 Ni-based superalloy fabricated with selective Laser melting (SLM). *Metals* **10**(5), 629.

Ding Y, Muñiz-Lerma JA, Trask M, Chou S, Walker A & Brochu M (2016). Microstructure and mechanical property considerations in additive manufacturing of aluminum alloys. *MRS Bull* **41**(10), 745–751.

Frazier WE (2014). Metal additive manufacturing: A review. *J Mater Eng Perform* **23**(6), 1917–1928.

Greer JR & Nix WD (2006). Nanoscale gold pillars strengthened through dislocation starvation. *Phys Rev B* **73**(24), 245410.

Haque MA & Saif MTA (2002). In-situ tensile testing of nano-scale specimens in SEM and TEM. *Exp Mech* **42**(1), 123–128.

Haque MA & Saif MTA (2004). Deformation mechanisms in free-standing nanoscale thin films: A quantitative in situ transmission electron microscope study. *Proc Natl Acad Sci U S A* **101**(17), 6335–6340.

Hilaire A, Andrieu E & Wu X (2019). High-temperature mechanical properties of alloy 718 produced by laser powder bed fusion with different processing parameters. *Addit Manuf* **26**, 147–160.

Imrich PJ, Kirchlechner C, Kiener D & Dehm G (2015). Internal and external stresses: In situ TEM compression of Cu bicrystals containing a twin boundary. *Scr Mater* **100**, 94–97.

Kelly SM & Kampe SL (2004). Microstructural evolution in laser-deposited multilayer Ti-6Al-4V builds: Part I. Microstructural characterization. *Metall Mater Trans A* **35**(6), 1861–1867.

Kiener D & Minor AM (2011). Source truncation and exhaustion: Insights from quantitative in situ TEM tensile testing. *Nano Lett* **11**(9), 3816–3820.

Kiener D, Motz C, Rester M, Jenko M & Dehm G (2007). FIB damage of Cu and possible consequences for miniaturized mechanical tests. *Mater Sci Eng A* **459**(1), 262–272.

Kuo Y-L, Horikawa S & Kakehi K (2017*a*). The effect of interdendritic δ phase on the mechanical properties of alloy 718 built up by additive manufacturing. *Mater Des* **116**, 411–418.

Kuo Y-L, Horikawa S & Kakehi K (2017*b*). Effects of build direction and heat treatment on creep properties of Ni-base superalloy built up by additive manufacturing. *Scr Mater* **129**, 74–78.

Kushima A, Huang JY & Li J (2012). Quantitative fracture strength and plasticity measurements of lithiated silicon nanowires by in situ TEM tensile experiments. *ACS Nano* **6**(11), 9425–9432.

Legros M, Gianola DS & Motz C (2011). Quantitative in situ mechanical testing in electron microscopes. *MRS Bull* **35**(5), 354–360.

Li H, Jia D, Yang Z, Liao X, Jin H, Cai D & Zhou Y (2021). Effect of heat treatment on microstructure evolution and mechanical properties of selective laser melted Ti–6Al–4 V and TiB/Ti–6Al–4 V composite: A comparative study. *Mater Sci Eng A* **801**, 140415.

Li W, Li S, Liu J, Zhang A, Zhou Y, Wei Q, Yan C & Shi Y (2016). Effect of heat treatment on AlSi10Mg alloy fabricated by selective laser melting: Microstructure evolution, mechanical properties and fracture mechanism. *Mater Sci Eng A* **663**, 116–125.

Li XP, Wang XJ, Saunders M, Suvorova A, Zhang LC, Liu YJ, Fang MH, Huang ZH & Sercombe TB (2015). A selective laser melting and solution heat treatment refined Al–12Si alloy with a controllable ultrafine eutectic microstructure and 25% tensile ductility. *Acta Mater* **95**, 74–82.

Lin T-C, Cao C, Sokoluk M, Jiang L, Wang X, Schoenung JM, Lavernia EJ & Li X (2019). Aluminum with dispersed nanoparticles by laser additive manufacturing. *Nat Commun* **10**(1), 4124.

Liu JF, Yang ZQ & Ye HQ (2015). In situ transmission electron microscopy investigation of quasicrystal-crystal transformations in Mg–Zn–Y alloys. *J Alloys Compd* **621**, 179–188.

Liu L, Ding Q, Zhong Y, Zou J, Wu J, Chiu Y-L, Li J, Zhang Z, Yu Q & Shen Z (2018). Dislocation network in additive manufactured steel breaks strength–ductility trade-off. *Mater Today* **21**(4), 354–361.

McKeown JT, Zweiacker K, Liu C, Coughlin DR, Clarke AJ, Baldwin JK, Gibbs JW, Roehling JD, Imhoff SD, Gibbs PJ, Tourret D, Wiezorek JMK & Campbell GH (2016). Time-resolved in situ measurements during rapid alloy solidification: Experimental insight for additive manufacturing. *JOM* **68**(3), 985–999.

Minor AM, Syed Asif SA, Shan Z, Stach EA, Cyrankowski E, Wyrobek TJ & Warren OL (2006). A new view of the onset of plasticity during the nanoindentation of aluminium. *Nat Mater* **5**(9), 697–702.

Mostafa A, Picazo Rubio I, Brailovski V, Jahazi M & Medraj M (2017). Structure, texture and phases in 3D printed IN718 alloy subjected to homogenization and HIP treatments. *Metals* **7**(6), 196.

Mumtaz KA, Erasenthiran P & Hopkinson N (2008). High density selective laser melting of Waspaloy®. *J Mater Process Technol* **195**(1), 77–87.

Popovich VA, Borisov EV, Popovich AA, Sufiiarov VS, Masaylo DV & Alzina L (2017). Impact of heat treatment on mechanical behaviour of Inconel 718 processed with tailored microstructure by selective laser melting. *Mater Des* **131**, 12–22.

Rao GA, Kumar M, Srinivas M & Sarma DS (2003). Effect of standard heat treatment on the microstructure and mechanical properties of hot isostatically pressed superalloy Inconel 718. *Mater Sci Eng A* **355**(1), 114–125.

Rao JC, Diao HY, Ocelík V, Vainchtein D, Zhang C, Kuo C, Tang Z, Guo W, Poplawsky JD, Zhou Y, Liaw PK & De Hosson JTM (2017). Secondary

phases in $Al_xCoCrFeNi$ high-entropy alloys: An in-situ TEM heating study and thermodynamic appraisal. *Acta Mater* **131**, 206–220.

Shan ZW, Mishra RK, Syed Asif SA, Warren OL & Minor AM (2008). Mechanical annealing and source-limited deformation in submicrometre-diameter Ni crystals. *Nat Mater* **7**(2), 115–119.

Shen M-Y, Tian X-J, Liu D, Tang H-B & Cheng X (2018). Microstructure and fracture behavior of TiC particles reinforced Inconel 625 composites prepared by laser additive manufacturing. *J Alloys Compd* **734**, 188–195.

Sing SL, Huang S & Yeong WY (2020). Effect of solution heat treatment on microstructure and mechanical properties of laser powder bed fusion produced cobalt-28chromium-6molybdenum. *Mater Sci Eng A* **769**, 138511.

Song B, Dong S, Liu Q, Liao H & Coddet C (2014). Vacuum heat treatment of iron parts produced by selective laser melting: Microstructure, residual stress and tensile behavior. *Mater Des* **54**, 727–733.

Song B, Dong S, Zhang B, Liao H & Coddet C (2012). Effects of processing parameters on microstructure and mechanical property of selective laser melted Ti6Al4 V. *Mater Des* **35**, 120–125.

Song B, Zhao X, Li S, Han C, Wei Q, Wen S, Liu J & Shi Y (2015). Differences in microstructure and properties between selective laser melting and traditional manufacturing for fabrication of metal parts: A review. *Front Mech Eng* **10**(2), 111–125.

Strößner J, Terock M & Glatzel U (2015). Mechanical and microstructural investigation of nickel-based superalloy IN718 manufactured by selective laser melting (SLM). *Adv Eng Mater* **17**(8), 1099–1105.

Ter Haar GM, Becker TH & Blaine DC (2016). Influence of heat treatments on the microstructure and tensile behaviour of selective laser melting-produced TI-6AL-4V parts. *South African J Ind Eng* **27**, 174–183.

Thijs L, Van Humbeeck J & Kruth JP (2015). Processing AlSi10Mg by selective laser melting: Parameter optimisation and material characterisation. *Mater Sci Technol* **31**(8), 917–923.

Thijs L, Verhaeghe F, Craeghs T, Humbeeck JV & Kruth J-P (2010). A study of the microstructural evolution during selective laser melting of Ti–6Al–4 V. *Acta Mater* **58**(9), 3303–3312.

Topping M, Ungár T, Race CP, Harte A, Garner A, Baxter F, Dumbill S, Frankel P & Preuss M (2018). Investigating the thermal stability of irradiation-induced damage in a zirconium alloy with novel in situ techniques. *Acta Mater* **145**, 255–263.

Trosch T, Strößner J, Völkl R & Glatzel U (2016). Microstructure and mechanical properties of selective laser melted Inconel 718 compared to forging and casting. *Mater Lett* **164**, 428–431.

Tsai M-T, Chen Y-W, Chao C-Y, Jang JSC, Tsai C-C, Su Y-L & Kuo C-N (2020). Heat-treatment effects on mechanical properties and microstructure evolution of Ti-6Al-4V alloy fabricated by laser powder bed fusion. *J Alloys Compd* **816**, 152615.

Tucho WM, Cuvillier P, Sjolyst-Kverneland A & Hansen V (2017). Microstructure and hardness studies of Inconel 718 manufactured by selective laser melting before and after solution heat treatment. *Mater Sci Eng A* **689**, 220–232.

Vilaro T, Colin C, Bartout JD, Nazé L & Sennour M (2012). Microstructural and mechanical approaches of the selective laser melting process applied to a nickel-base superalloy. *Mater Sci Eng A* **534**, 446–451.

Vrancken B, Thijs L, Kruth J-P & Van Humbeeck J (2012). Heat treatment of Ti6Al4 V produced by selective laser melting: Microstructure and mechanical properties. *J Alloys Compd* **541**, 177–185.

Wang B & Haque MA (2015). In situ microstructural control and mechanical testing inside the transmission electron microscope at elevated temperatures. *JOM* **67**(8), 1713–1720.

Wang J, Zeng Z, Weinberger CR, Zhang Z, Zhu T & Mao SX (2015). In situ atomic-scale observation of twinning-dominated deformation in nanoscale body-centred cubic tungsten. *Nat Mater* **14**, 594.

Wang MS, Kaplan-Ashiri I, Wei XL, Rosentsveig R, Wagner HD, Tenne R & Peng LM (2008). In situ TEM measurements of the mechanical properties and behavior of WS2 nanotubes. *Nano Res* **1**(1), 22.

Wang Z, Guan K, Gao M, Li X, Chen X & Zeng X (2012). The microstructure and mechanical properties of deposited-IN718 by selective laser melting. *J Alloys Compd* **513**, 518–523.

Wang Z, Wu W, Qian G, Sun L, Li X & Correia JAFO (2019). In-situ SEM investigation on fatigue behaviors of additive manufactured Al-Si10-Mg alloy at elevated temperature. *Eng Fract Mech* **214**, 149–163.

Wu J, Wang XQ, Wang W, Attallah MM & Loretto MH (2016). Microstructure and strength of selectively laser melted AlSi10Mg. *Acta Mater* **117**, 311–320.

Zhang D, Niu W, Cao X & Liu Z (2015). Effect of standard heat treatment on the microstructure and mechanical properties of selective laser melting manufactured Inconel 718 superalloy. *Mater Sci Eng A* **644**, 32–40.

Zhang HY, Zhang SH, Cheng M & Li ZX (2010). Deformation characteristics of δ phase in the delta-processed Inconel 718 alloy. *Mater Charact* **61**(1), 49–53.

Zhang M, Yang Y, Song C, Bai Y & Xiao Z (2018). An investigation into the aging behavior of CoCrMo alloys fabricated by selective laser melting. *J Alloys Compd* **750**, 878–886.

Zhao X, Chen J, Lin X & Huang W (2008). Study on microstructure and mechanical properties of laser rapid forming Inconel 718. *Mater Sci Eng A* **478**(1), 119–124.

Zhou L, Mehta A, McWilliams B, Cho K & Sohn Y (2019). Microstructure, precipitates and mechanical properties of powder bed fused Inconel 718 before and after heat treatment. *J Mater Sci Technol* **35**(6), 1153–1164.

Zhu Y & Espinosa HD (2005). An electromechanical material testing system for in situ electron microscopy and applications. *Proc Natl Acad Sci U S A* **102**(41), 14503–14508.

Zhu Y, Moldovan N & Espinosa HD (2005). A microelectromechanical load sensor for in situ electron and x-ray microscopy tensile testing of nanostructures. *Appl Phys Lett* **86**(1), 013506.

Zweiacker K, McKeown JT, Liu C, LaGrange T, Reed BW, Campbell GH & Wiezorek JMK (2016). Determination of crystal growth rates during rapid solidification of polycrystalline aluminum by nano-scale spatio-temporal resolution in situ transmission electron microscopy. *J Appl Phys* **120**(5), 055106.

https://doi.org/10.1017/S1431927621000052 Published online by Cambridge University Press